This article was downloaded by:[Heitz, D.]
[Heitz, D.]
On: 6 June 2007
Access Details: [subscription number 779359604]
Publisher: Taylor & Francis
Informa Ltd Registered in England and Wales Registered Number: 1072954
Registered office: Mortimer House, 37-41 Mortimer Street, London W1T 3JH, UK

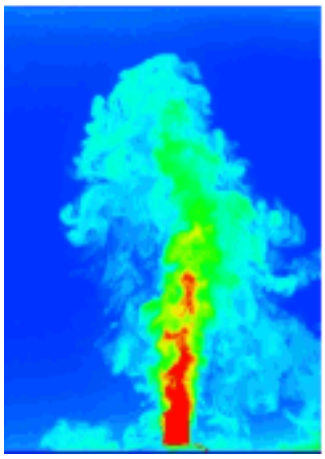

Journal of Turbulence
Publication details, including instructions for authors and subscription information:
http://www.informaworld.com/smpp/title~content=t713665472

Direct numerical simulations of vortex shedding behind cylinders with spanwise linear nonuniformity

To cite this Article: Parnaudeau, P., Heitz, D., Lamballais, E. and Silvestrini, J.-H. , 'Direct numerical simulations of vortex shedding behind cylinders with spanwise linear nonuniformity', Journal of Turbulence, 8:1, 1 - 13
To link to this article: DOI: 10.1080/14685240600767706
URL: http://dx.doi.org/10.1080/14685240600767706

PLEASE SCROLL DOWN FOR ARTICLE

Full terms and conditions of use: http://www.informaworld.com/terms-and-conditions-of-access.pdf

This article maybe used for research, teaching and private study purposes. Any substantial or systematic reproduction, re-distribution, re-selling, loan or sub-licensing, systematic supply or distribution in any form to anyone is expressly forbidden.

The publisher does not give any warranty express or implied or make any representation that the contents will be complete or accurate or up to date. The accuracy of any instructions, formulae and drug doses should be independently verified with primary sources. The publisher shall not be liable for any loss, actions, claims, proceedings, demand or costs or damages whatsoever or howsoever caused arising directly or indirectly in connection with or arising out of the use of this material.

© Taylor and Francis 2007

Journal of Turbulence
Volume 8, No. 13, 2007

Downloaded By: [Heitz, D.] At: 14:56 6 June 2007

Direct numerical simulations of vortex shedding behind cylinders with spanwise linear nonuniformity

P. PARNAUDEAU†‡, D. HEITZ†∗, E. LAMBALLAIS‡ and J.-H. SILVESTRINI¶

†Cemagref, 17 Avenue de Cucillé–CS64427, F35044 Rennes Cedex, France
‡Laboratoire d'Études Aérodynamiques, ENSMA, CNRS UMR 6609, Université de Poitiers, Téléport 2-Bd. Marie et Pierre Curie B.P. 30179, 86962 Futuroscope Chasseneuil Cedex, France
¶Departamento de Engenharia Mecânica e Mecatrônica, Faculdade de Engenharia, Pontificia Universidade Catolica do Rio Grande do Sul, Av. Ipiranga 6681, 90619-900 Porto Alegre—RS, Brasil

Three-dimensional direct numerical simulations of vortex shedding behind cylinders have been performed when the body diameter and the incoming flow involved spanwise linear nonuniformity. Four configurations were considered: the shear flow, the tapered cylinder and their combination which gave rise to namely the adverse and aiding cases. In contrast with the observations of other investigators, these computations highlighted distinct vortical features between the shear case and the tapered case. In addition, it was observed that the shear case and the adverse case (respectively tapered case and aiding case), yielded similarities in flow topology. This phenomenon was explained by the spanwise variations of U/D which seemed to govern these flows. Indeed, it was observed that large spanwise variations of U/D seemed to enhance three dimensionality, through the appearance of vortex adhesions and dislocations. Spanwise cellular pattern of vortex shedding was identified. Their modifications in cell size, junction position and number were correlated with the variation of U/D. In the lee side of the obstacle a wavy secondary motion was identified. Induced secondary flow due to the bending of Karman vortices in the vicinity of vortex adhesion and dislocations was suggested to explain this result.

Keywords: Direct numerical simulation; Wake; Circular cylinder; Tapered cylinder; Shear flow

1. Introduction

Three-dimensional vortex shedding is a common feature in many engineering applications such as marine risers, heat exchangers or ultra-clean protection devices in the food industry. In the absence of spanwise nonuniformities and end effects, three-dimensional flow behavior occurs as an intrinsic feature of vortex wakes, governed by the Reynolds number [21] or by the bending of yawed cylinders [23]. However, complex wake flows encountered in engineering applications usually involve spanwise nonuniformity of the body diameter D and/or of the oncoming flow U. For variations of the oncoming flow (shear flow) or of the cylinder diameter (tapered cylinder, stepped cylinder) the flow exhibits common features such as cells of constant frequency, oblique shedding and vortex dislocations (see, e.g., [3, 4, 11, 14–16, 24] for shear flows [1, 6, 7, 18, 20, 26], for tapered cylinders [13, 25], for stepped cylinder). For linear variations of the oncoming flow (constant shear flow) or of the cylinder diameter (linearly tapered cylinder) the flows are considered to be similar in behavior. Indeed, in both cases, U/D and UD change along the span of the cylinder. Nevertheless, when for a shear flow U/D

*Corresponding author. E-mail: dominique.heitz@cemagref.fr

Journal of Turbulence
ISSN: 1468-5248 (online only) © 2007 Taylor & Francis
http://www.tandf.co.uk/journals
DOI: 10.1080/14685240600767706

Downloaded By: [Heitz, D.] At: 14:56 6 June 2007

and *UD* spanwise distributions are similar, for a tapered cylinder these profiles are opposed. In addition, for linear shear flow the base pressure gradients lead to secondary flow [29], whereas for tapered cylinder the base pressure is nearly constant without secondary motion [25]. Therefore, the two wakes experience distinct spanwise flow mechanisms. Surprisingly, they are considered to be similar in behavior [2, 7, 13, 25]. This viewpoint is mainly explained in the light of the cellular vortex shedding that both flows share. Moreover, when linear nonuniform oncoming flow is combined with linear nonuniform cylinder the wake flows experience two opposed effects. In one case, in which the maximum velocity corresponds to the large diameter end of the cylinder, the spanwise distribution of *UD* is enhanced whereas U/D remains constant. In the other case, in which the maximum velocity corresponds to the small diameter end of the cylinder, the spanwise distribution of *UD* lies in a narrow range whereas U/D is enhanced. Considering the effect of the shear, [2] explained that in one case, called adverse, the shear cancels the taper, whereas in the other case, called shear aiding taper, the shear aids the taper. In the following we use the name adverse case when the variations of U/D are canceled, and the name aiding case when they are enhanced.

The aim of this study is to analyze the spanwise dynamical organization and compare the flow topology of the wake behind a circular cylinder in a constant shear flow with the wake of a linearly tapered circular cylinder. Furthermore, in the light of the vortical organization of these two flows, the responses of the wakes which combine both involved spanwise nonuniformities are investigated. In the present study, the spanwise *UD* or Reynolds number variations induced by the nonuniformities span the laminar-transitional and turbulent flow regimes for wakes. Particular attention was paid to the spanwise coexistence of these flow regimes. The spanwise transitioning was compared to the scenario observed for circular cylinder in uniform flow. The three-dimensional instability modes depending on the regime of the Reynolds number and scaling on the primary vortices or streamwise vortices were identified. Hence, the spanwise transition to turbulence was addressed for cylinder with linear spanwise nonuniformities.

After a short presentation of the four flow configurations considered, some details about the numerical methods are presented. Then, using visualizations, it is shown that the shear case and the taper case exhibit distinct features, whereas not only the shear case and the adverse case but also the tapered case and the aiding case, yield similar flow topology. In the three last sections, these observations are discussed from the analysis of the wake transition, secondary flows and frequency variations along the span of the cylinders.

2. Flow configuration and parameters

Uniform and shear flows over circular and tapered cylinder are considered in a Cartesian frame of reference $\Gamma = (0; x; y; z)$, where the cylinder axis is oriented along the vertical direction y at the intersection between the streamwise section x_{cyl} and the spanwise one $z = 0$ (see figure 1). In the case of tapered cylinder, in the interval $-L'_y/2 < y < L'_y/2$, the profile of the diameter $D(y)$, at $x = x_{\mathrm{cyl}} = 7D_c$, is given by

$$D(y) = \frac{D_1 + D_2}{2} + \frac{D_2 - D_1}{12}\frac{D_c}{L'_y}\left\{\ln\left(\frac{\cosh\left[\frac{6}{D_c}\left(y + \frac{L'_y}{2}\right)\right]}{\cosh\left[\frac{6}{D_c}\left(y - \frac{L'_y}{2}\right)\right]}\right)\right\}, \tag{1}$$

where $D_c = (D_1 + D_2)/2$ is the median diameter. Outside this interval the diameter is constant and equal to D_1 (for $y < -L'_y/2$) and to D_2 (for $y > L'_y/2$), with $D_1 > D_2$. Note that in the case of a circular cylinder the diameter is D_c.

Downloaded By: [Heitz, D.] At: 14:56 6 June 2007

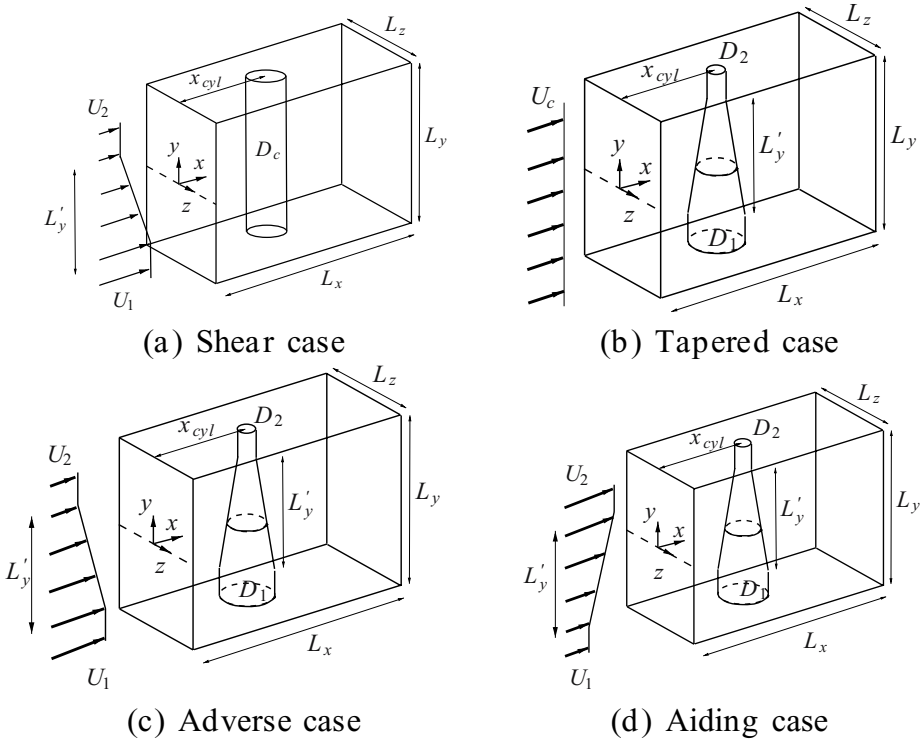

Figure 1. Schematic views of the flow configurations.

At the inflow section, uniform or shear flows are considered. The shear flow is aligned in the y-direction and extended in a zone $-L'_y/2 < y < L'_y/2$. Outside this interval two streams of constant velocities U_1 and U_2 are imposed. The inflow velocity profile $U(y)$ at $x = 0$ reads

$$U(y) = \frac{U_1 + U_2}{2} + \frac{U_2 - U_1}{12}\frac{D_c}{L'_y}\left\{\ln\left(\frac{\cosh\left[\frac{6}{D_c}\left(y + \frac{L'_y}{2}\right)\right]}{\cosh\left[\frac{6}{D_c}\left(y - \frac{L'_y}{2}\right)\right]}\right)\right\}, \tag{2}$$

without any additional perturbations (steady inflow condition). In the case of a uniform flow, the inflow velocity profile is the median velocity, given by $U_c = (U_1 + U_2)/2$. Note that the shape of the stream velocity is the same as the shape of the cylinder. This shape allows us to consider a constant shear flow extending on a wide region while preserving the free-slip conditions imposed at $y = \pm L_y/2$. As is reported in the paper of [24], the presence of free-slip walls imposes a kinematic blocking associate with the condition $u_y(x, \pm L_y/2, z) = 0$. Note finally that a periodic boundary condition is imposed in the z-direction. The simulations are performed by considering two parameters, the shear parameter β_U and the tapered parameter β_D. β_U and β_D are defined by

$$\beta_U = -\frac{D_c}{U_c}\frac{\mathrm{d}U}{\mathrm{d}y} \quad \text{and} \quad \beta_D = -\frac{D_2 - D_1}{L'_y}. \tag{3}$$

The couple $(\beta_U,\ L'_y)$ and $(\beta_D,\ L'_y)$ are considered with $U_1 = 3U_c/2$, $U_2 = U_c/2$—except for the aiding case where $U_1 = U_c/2$, $U_2 = 3U_c/2$—and with $D_1 = 3D_c/2$, $D_2 = D_c/2$

Downloaded By: [Heitz, D.] At: 14:56 6 June 2007

Table 1. Flow configurations.

Case	Re_1	Re_2	L'_y	β_U	β_D
Shear	300	100	$40D_c$	0.025	0
Tapered	300	100	$40D_c$	0	0.025
Adverse	900	100	$40D_c$	0.025	0.025
Aiding	150	150	$40D_c$	−0.025	0.025

for all configurations. The corresponding Reynolds number values at both extremities $\mathrm{Re}_1 = U_1 D_1/\nu$ and $\mathrm{Re}_2 = U_2 D_2/\nu$ are given in table 1. The midspan Reynolds number is equal to 200, except in the aiding case where the midspan Reynolds is equal to 400.

The shear flow and the tapered cylinder have the same profile of Reynolds number, ranging from $\mathrm{Re}_1 = 300$ to $\mathrm{Re}_2 = 100$ along the span of the cylinder. The aiding case has symmetric Reynolds number spanwise distribution, with a maximum equal to 200 at midspan, and a minimum equal to $\mathrm{Re}_1 = \mathrm{Re}_2 = 150$ at both extremities. For the adverse case, the Reynolds number exhibits a parabolic spanwise distribution for $-L'_y/2 < y < L'_y/2$ ranging from $\mathrm{Re}_1 = 900$ to $\mathrm{Re}_2 = 100$.

3. Numerical method

The incompressible Navier–Stokes equations are directly solved in a computational domain $L_x \times L_y \times L_z = 22D_c \times 48D_c \times 12D_c$ discretized on a Cartesian, regular and non-staggered grid of $n_x \times n_y \times n_z = 397 \times 385 \times 216$ points.[1] Sixth-order compact centred difference schemes are used to evaluate all spatial derivatives except near the inflow and outflow sections where x-derivatives are calculated using fourth- (Pade) and third-order (single-sided) compact schemes. The outflow boundary condition consists in solving a simplified linear equation of convective nature for the velocity. Time integration is performed with a second-order Adams–Bashforth scheme. For the full advancement of a time step, the zero divergence condition is ensured by a projection method through the resolution of a Poisson-like equation based on a direct solver. For more details about the numerical code, see [11, 12].

The no-slip condition at the cylinder surface is imposed via an immersed boundary method. In the present flow configuration where the main directions of the cylinder shape are not aligned on the main directions of the flow, the use of an immersed boundary approach is very simple and computationally efficient because this technique does not require the grid to fit the body surface. Here, we use a direct forcing technique specifically developed to be favorably combined with a spatial discretization based on high-order schemes. Basically, the principle of this method is to calibrate the forcing to ensure the no-slip condition at the cylinder surface while creating an artificial flow (with a mass source/sink) inside the body in order to preserve the regularity of the velocity field across the immersed boundary. Comparing DNS data of a flow over a circular cylinder at a Reynolds number similar to here [19], have shown that this procedure leads to a significant improvement of results both qualitatively and quantitatively.

[1] Taking the Reynolds number into account, the DNS of the Adverse case can be considered as being spatially under-resolved compared to the other calculations.

Downloaded By: [Heitz, D.] At: 14:56 6 June 2007

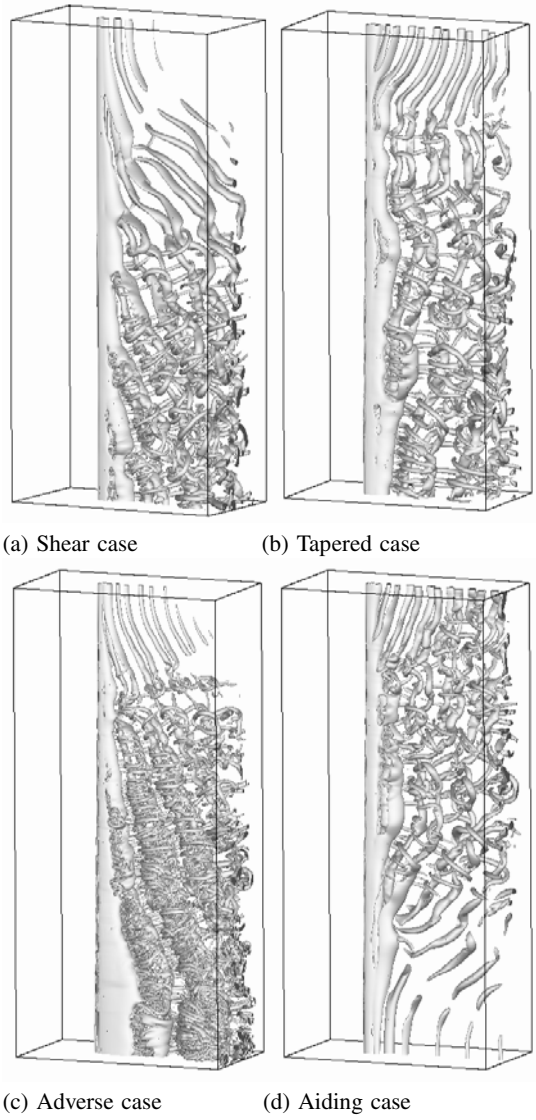

(a) Shear case (b) Tapered case

(c) Adverse case (d) Aiding case

Figure 2. Perspective views showing isosurfaces of the second invariant (Q) of velocity gradient tensor $Q = 0.2U_c^2/D_c^2$ for $t = 75D_c/U_c$.

4. Results and discussion

4.1 *Instantaneous vortex pattern*

Perspective views of instantaneous isosurfaces of the second invariant $Q = (\Omega_{ij}\Omega_{ij} - S_{ij}S_{ij})/2$ of the velocity gradient tensor are shown in figure 2. The choice of the Q criterion has been made to visualize vortex cores by avoiding the detection of vorticity sheets. It was observed that all flows shared primary von-Karman vortices, longitudinal vortices, oblique shedding, and pockets of dislocations.[2]

[2] Animations (mpeg format) are available on the internet link http://labo.univ-poitiers.fr/informations-lea/tsfp4paper/index.htm

Downloaded By: [Heitz, D.] At: 14:56 6 June 2007

Examination of figure 2 shows that despite the fact that the shear flow configuration and the tapered configuration are considered to be quite similar in behavior, both configurations exhibited distinct features. Furthermore, it was noted that the shear case and the adverse case (respectively tapered case and aiding case), yielded similar flow topology. Indeed, the shear and adverse flow cases indicated oblique vortex shedding distribution along the span of the cylinder, with increasing slant further downstream. As observed in the experiments on the flow past cylinder in shear flow by [10], the vortices spread fan-like. In the very near wake, the angle of the vortex shedding is related to the incoming shear and to the vortex shedding propagation along the span of the cylinder, whereas further downstream the obliqueness is increased by the advection [24]. In contrast, the tapered case and the aiding case yielded less regular oblique shedding vortices with spanwise and temporal variations. This phenomenon which may be linked with large spanwise variations of U/D, leading to large spanwise variations of the vortex shedding frequency, will be explained in the following sections. In addition, due to the constant spanwise distribution of U/D, the adverse case displayed vortex shedding with large spanwise coherence, compared to the other configurations exhibiting vortex splitting into cells of approximately constant shedding angle. All these phenomena will be discussed in further detail in the following sections.

4.2 *Spanwise wake transition*

The distributions of Reynolds number associated with the spanwise nonuniformity, of the inflow velocity profile and of the cylinder diameter, are shown in figures 3(a), 4(a), 5(a) and 6(a).

The wake of two-dimensional cylinders in uniform streams has been extensively studied. For the laminar regime ($50 < \mathrm{Re} < 190$) and for the turbulent regime $260 < \mathrm{Re} < 5000$, the flow is sensitive to end conditions and parallel shedding mode can be imposed. Whereas for the wake transition regime ($190 < \mathrm{Re} < 250$), the vortex shedding cannot be controlled via boundary manipulations and spontaneous vortex dislocations appear. It is generally considered that the

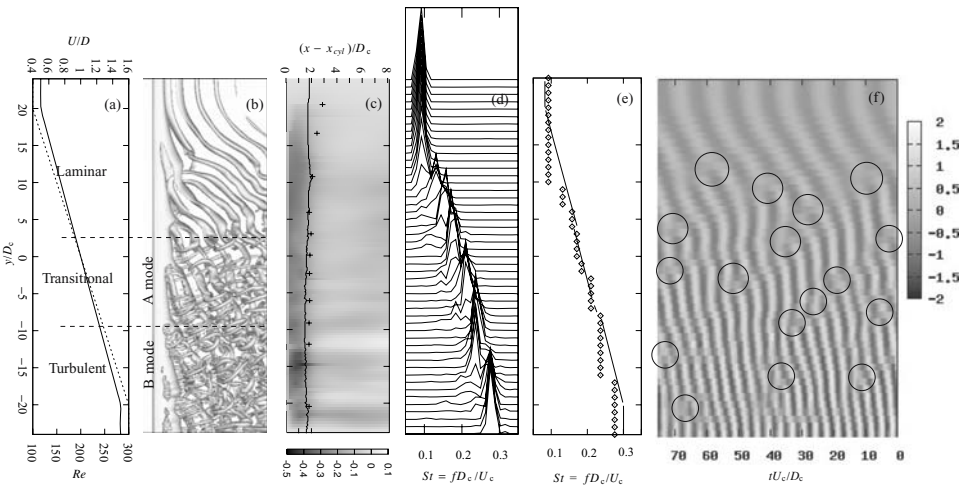

Figure 3. Spanwise distributions in the near wake of the shear case: (a) U/D (–) and Re (– –); (b) Instantaneous isosurface of $Q = 0.2U_c^2/D_c^2$ at $t = 75D_c/U_c$; (c) spanwise mean velocity component (grey level) and formation length (+, Williamson (1996) measurements; ○, Gerrard (1978) measurements); (d) spanwise variation of frequency spectra of the transverse velocity component monitored at $(x - x_{\mathrm{cyl}})/D_c = 1$ and $z = 0$; (e) Strouhal number (◇, present simulations; –, Fey *et al.* (1998) laws); (f) spatiotemporal variations of the transverse velocity along the span of the cylinder.

Downloaded By: [Heitz, D.] At: 14:56 6 June 2007

transition to three dimensionality involves two discontinuities in the Strouhal–Reynolds curve which are linked with two instabilities [28]. The mode A instability, whose onset is about $\mathrm{Re} = 190$, is characterized by a spanwise wavelength of about four diameters, associated with streamwise vortices in the Karman street. The mode B instability, whose onset is around $\mathrm{Re} = 230$ and which becomes dominant from $\mathrm{Re} = 260$, is characterized by finer scale like streamwise vortices between Karman vortices with a wavelength of about one diameter. Furthermore, under strong perturbations (i.e. for cylinder with finite aspect ratio in experiments [27], or strong inhomogeneities in the initial conditions in simulations [30]), vortex-adhesion mode appears for $160 < \mathrm{Re} < 230$ and is characterized by spot-like vortex deformations.

In the present flow configurations the aforementioned regimes (laminar, transitional and turbulent) and modes (vortex-adhesion, A and B) were identified. Indeed, for the four flows, the three regimes and the three modes (vortex-adhesion, A and B) coexisted along the span. In figures 3(a), 4(a), 5(a) and 6(a), horizontal dashed lines, corresponding to the Reynolds number regime boundaries for two-dimensional cylinders in uniform streams, are marked. For the shear and adverse cases the regimes and modes were retrieved at the same Reynolds number values as for uniform wake flow. In figure 5(b), for the adverse case, one adhesion point was clearly observed at $y/D_c \simeq 12$ (i.e. in the transitional regime). In contrast for the tapered (figure 4) and the aiding (figure 6) cases, vortex-adhesion mode and mode A were observed in the laminar regime where U/D experienced large variations. In addition, for the tapered (figure 4) and the aiding (figure 6) cases vortex-adhesions appeared more often in time and space along the span of the cylinder than for the shear (figure 3) and the adverse (figure 5) cases. This mechanism was responsible of the temporal variations of the oblique shedding angle of the vortices. In the animation of the adverse case, based on the whole image sequence (i.e. $T = 75D_c/U_c$), a similar vortex sticking phenomenon was identified, at $y/D_c \simeq -8$, from the middle of the image sequence to the end. Due to its spontaneous appearance and persistence, this particular adhesion point seemed to be self-sustaining. Interestingly, for the four wake flow considered, adhesion mode appeared even at Reynolds number higher than 230 which is considered to be the upper limit for two-dimensional cylinder in uniform flow [30].

The above general behavior suggests that the spanwise nonuniformity characterized by strong variations of U/D induced the appearance of vortex-adhesion mode and of dislocations, hence increasing the transition to three dimensionality. As a result the configurations dominated by the incoming shear flow (i.e. the shear flow and the adverse flow) were different in behavior to those influenced by the taper of the cylinder (i.e. the tapered and the aiding).

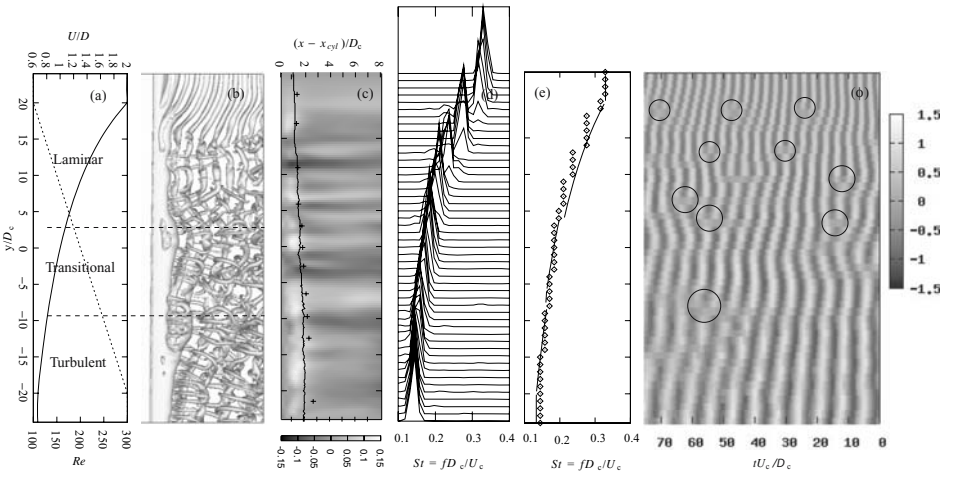

Figure 4. Spanwise distributions in the near wake of the tapered case (see figure 3 for details).

Downloaded By: [Heitz, D.] At: 14:56 6 June 2007

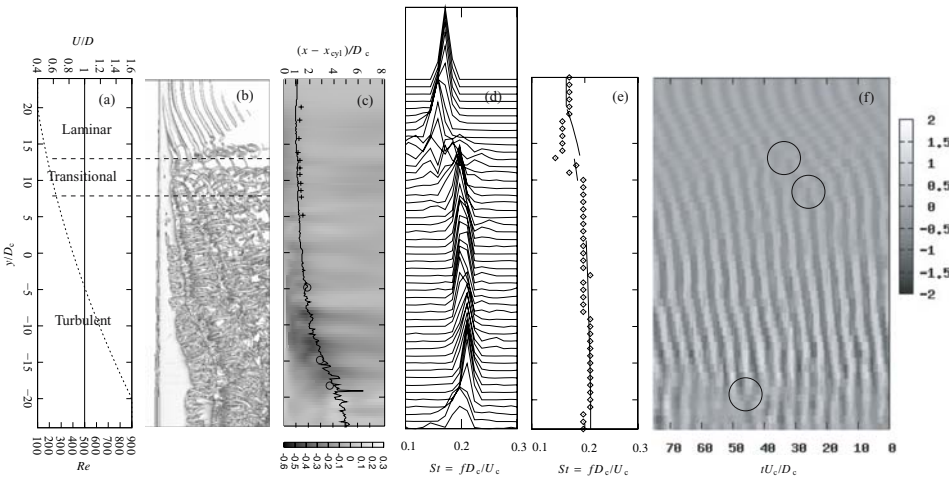

Figure 5. Spanwise distributions in the near wake of the adverse case (see figure 3 for details).

4.3 *Frequency analysis*

Figures 3(d), 4(d), 5(d) and 6(d) show the spanwise variation of frequency spectra of the transverse velocity. The spanwise distributions of the Strouhal number, corresponding to the maxima of the spectra, are plotted in figures 3(e), 4(e), 5(e) and 6(e). For the four cases these frequency distributions were scaled on the variation of U/D. However, since these Strouhal number were not determined with long-time average spectrum (around 15 vortex shedding cycles at the midspan), their distributions were not smooth and the organization of the wakes exhibited cells of constant frequency. The width of the cells increased with decreasing values of the variations of U/D, which was consistent with [9] and [20] findings—increasing cells with decreasing β—reported for a circular cylinder in a shear flow and for a tapered cylinder in uniform flow, respectively. For the tapered case, we extrapolated the results of [20], obtained for a midspan Reynolds number ranging from 100 to 145 and for a taper parameter ranging from 0.01 to 0.02. The number of shedding cells for all the cylinders (N) with respect to the taper parameter matched the following linear distribution: $N \simeq 300\beta$. For the tapered case

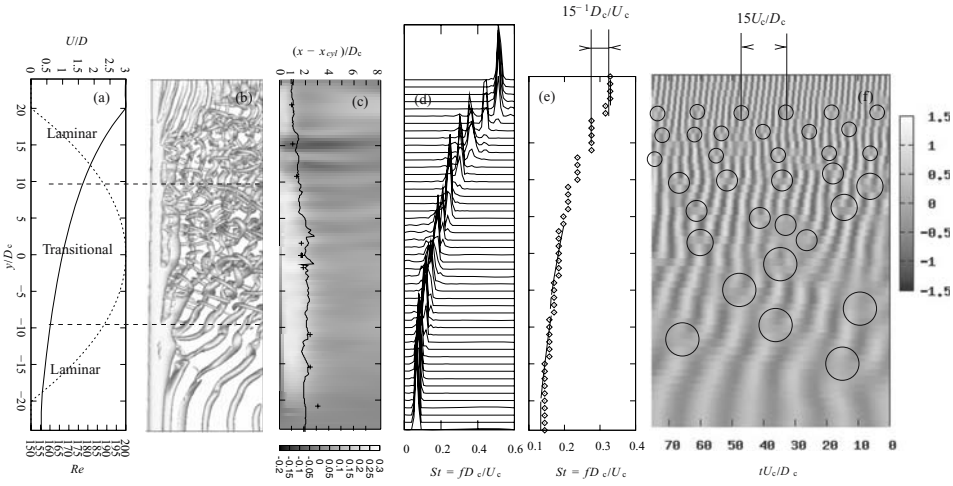

Figure 6. Spanwise distributions in the near wake of the aiding case (see figure 3 for details).

Downloaded By: [Heitz, D.] At: 14:56 6 June 2007

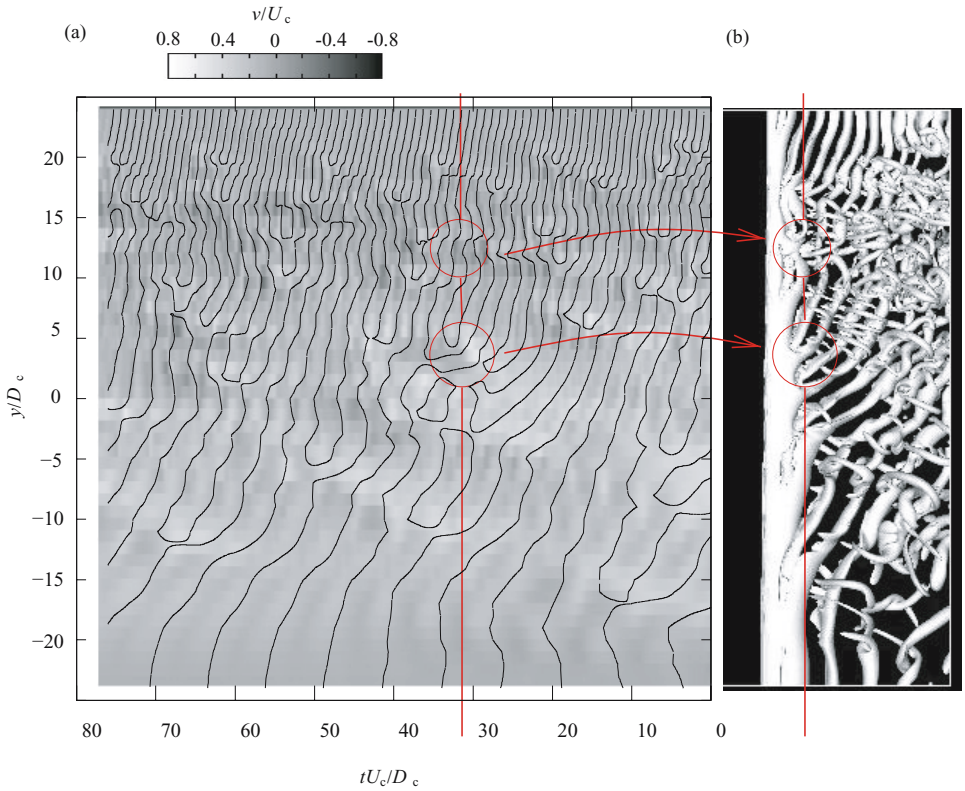

Figure 7. Secondary flow linked with dislocation and vortex-adhesion mode for the aiding case: (a) gray level of the spatiotemporal spanwise velocity component and spatiotemporal isolevels of zero transverse velocity component; (b) instantaneous isosurface $Q = 0.2U_c^2/D_c^2$ at $t = 32D_c/U_c$.

considered in the present study, i.e. with a midspan Reynolds number of 200 and a taper parameter of 0.025, the number of cells calculated with this model was around 7.5, which was consistent with the data plotted in figure 4. In addition, the non-dimensionalized mean cell length recast in terms of the steepness parameter, reads $L'_y/N \times \beta$, and was equal to 0.133, in excellent agreement with the results of [20].

For the adverse case, as there was no variation of U/D, only a single cell was expected. However, results yielded a Strouhal discontinuity corresponding to the spanwise region where the laminar regime gave way to the inception of vortex-adhesion modes, mode A and mode B (i.e. the transitional regime). Around $y/D_c \simeq -8$ another discontinuity in spanwise Strouhal distribution was also related with the presence of a vortex-adhesion mode. In general for the four configurations considered, discontinuous variations in the spanwise frequency distribution were correlated with vortex-adhesion mode or vortex phase break up at their junctions. As already observed in previous studies, the cellular pattern of vortex shedding is an adjustment of the vortex shedding frequency to the spanwise nonuniformity. Nevertheless, depending on different parameters (L/D, β and Re) leading to important scatter in cells position and size, nearly continuous frequency distributions may be observed, although cells exist in the instantaneous flow visualizations [10]. Based on spatiotemporal analysis to observe the transient movement of the cells boundaries [16], conjectured that the frequency spectra alone might not be the best indicator of the cellular shedding pattern. Recently [22], showed that the FFT analysis of the signal is not sufficient and that the spanwise frequency distribution is more complex than the classical cellular description in discrete steps. In the present cases, the

Downloaded By: [Heitz, D.] At: 14:56 6 June 2007

cellular appearance may be also due to the limitations of the FFT analysis over a short time period.

In order to have further insight in the transition of the frequency between cells, spatiotemporal variations of the transverse velocity along the span of the cylinder are presented in figures 3(f), 4(f), 5(f) and 6(f). In these representations the continuous bright region can be considered as the footprints of the vortex line, as there is a link between the maximum of velocity and the passing of the vortices. For all configurations, the dislocations have been marked with circles. Results indicated that vortex dislocations appeared in the vicinity of the boundaries of the cells. Depending on the spanwise variation of U/D, the junctions between cells—determined from the spanwise location of the dislocations—seemed to be more or less diffuse. For large (respec. small) variations of U/D the dislocations exhibited transient movement in a narrow (respec. wide) spanwise range. In addition large variation of U/D gave rise to narrower cells compared to the spanwise region with small variation of U/D. Indeed for large variation of U/D large spanwise phase coherence of the Karman vortices is difficult to attempt. As a consequence, the number of cells along the span was higher for configurations with large spanwise variations of U/D. It is worth noting that the frequency of appearance of the dislocations was equal to the beating frequency of two neighboring cells. For instance for the aiding case at $y/D_c \simeq 20$ the inverse of the difference of frequency between the two cells $(0.515 - 0.449)^{-1} \simeq 15U_c/D_c$ was nearly equal to the time period measured between two dislocations. At this stage we can easily observe in the region with slight variations of U/D, that much longer time integration would be needed to obtain statistically converged spectrum. Indeed for the adverse and tapered cases only one dislocation can be observed in these spanwise regions.

The slope of the time traces of the transverse velocity is equal to the velocity propagation of the vortex shedding along the cylinder. In addition [24], suggested that the angle of the vortex shedding is directly linked with the characteristic speed of the vortex shedding propagation. Present results indicated a spatio-temporal variation of the angle of the vortex shedding around mean values. In particular, due to vortex-adhesion mode, negative and positive vortex shedding angles (with respect to the vertical zero angle) coexisted along the span of the body. The mean angles were determined from a scaling of the Strouhal laws, proposed by [5], by the cosine variations along the span. The piecewise model used is expressed as

$$St(y) = \frac{U(y)\cos\theta}{D(y)}(St^{\star} + m/\sqrt{\mathrm{Re}}),$$

where θ is mean angle, $St^{\star}$ and m are coefficients depending on the Reynolds number interval considered (see [5]). For $\theta = 0$, this expressions gives the relationships of [5], plotted in figures 3(e), 4(e), 5(e) and 6(e). It appeared that the mean angles found were consistent with the measurements made directly in the views of the instantaneous isosurface of the Q criterion. Spatiotemporal observations of the velocity components showed a more complex vortex pattern than the cellular structure with fixed junctions obtained with FFTs. Most probably, for long-time averaged spectrum the information of non-fixed dislocations, leading to diffuse cells, should be contained into the broadening of the peak of frequency.

4.4 *Secondary flows and formation length*

An important feature of the shear flow is the presence of a secondary flow in the lee side due to the base pressure gradient [16, 29]. In contrast, the wake over a tapered cylinder in a uniform flow, exhibits roughly constant base pressure along the span and no secondary motions are observed [25].

Downloaded By: [Heitz, D.] At: 14:56 6 June 2007

Figures 3(c), 4(c), 5(c) and 6(c) show the isovalues of the spanwise mean velocity component. As expected, results indicated that the three configurations involving a linear incoming velocity profile had a spanwise flow toward the high velocity end. However, for the four flow configurations considered, the spanwise secondary motion exhibited wavy distributions. Surprisingly, the tapered cylinder in a uniform flow, yielded a more pronounced cellular distribution of the spanwise mean velocity, dominated by cells of motion toward the small diameter end. These wavy distributions of the secondary motions may be related to the three dimensionalities induced by the adhesion points. Indeed, close examination of the animation showed that the region of reverse spanwise velocity experienced an adhesion mode. Figure 7 illustrates this phenomenon for the aiding case. Indeed, the spanwise velocity component was plotted in greylevels, and isovalues of zero transverse velocity were added to exhibit distinctly vortex adhesions and dislocations. One vortex adhesion and one pocket of dislocations were highlighted at, respectively, $y/D_c \simeq 13$ and $y/D_c \simeq 4$, for $t \simeq 32D_c/U_c$. This figure shows that in the vicinity of the vortex adhesion Karman vortices were bent toward an anticlockwise angle associated with negative spanwise velocity component, whereas for the pocket of dislocations, Karman vortices were bent toward a clockwise angle associated with a positive spanwise velocity component. At this stage we suggest that the wavy distributions of the spanwise velocity component may be induced by the obliqueness of the vortex shedding. This point needs further insight.

Figures 3(c), 4(c), 5(c) and 6(c) show the spanwise distribution of the formation length. Measurements of [28] and [8] were also plotted in these figures. In the present study, the characteristic length of the near wake formation region was obtained from the distance between the cylinder axis and the streamwise coordinate of the points, on the wake centreline, where the r.m.s. of the streamwise velocity has reached a maximum [28], determined this length from the distance between the cylinder axis and the streamwise coordinate of the points, on each side of the wake, where the r.m.s. of a single hot-wire cooling velocity has reached a maximum [8], determined the formation length from the point closest to the cylinder at which irrotional fluid crosses the wake centreline (flow visualization). All these definitions are compatible and provide comparable vortex formation distances [17]. Results indicated that the secondary flow took place in the recirculation zone. In addition comparisons with the experiments of [28] and [8] showed that the spanwise wake transition influenced the formation length as does the Reynolds number for two-dimensional cylinder in uniform flow. For each configuration some discrepancies were observed at the one end of the cylinder. This phenomenon, which needs further insight, may be due to a blockage effect induced by the secondary flow toward the free-slip wall. At these locations the Strouhal number yielded larger values than for a two-dimensional cylinder in a uniform flow.

5. Conclusion

In the present study we, have analyzed and compared the spanwise dynamical organizations of wakes behind a cylinder in a constant shear flow (shear case), behind a tapered cylinder in a uniform flow (tapered case), and behind the two combinations of these spanwise nonuniformities (adverse and aiding cases). In order to perform the direct numerical simulations of these complex flows, an immersed boundary method developed for a compact scheme was used.

Although considered to be similar in behavior, visualizations showed that the shear case and the tapered case had distinct features. The shear case and the adverse case yielded similar flow topology with oblique vortex shedding distributions along the span. In contrast, the tapered case and the aiding case experienced less regular oblique shedding vortices with spanwise and

Downloaded By: [Heitz, D.] At: 14:56 6 June 2007

temporal variations. These characteristics were explained by the spanwise variations of U/D governing these flows. Large spanwise variations of U/D seemed to enhance the transition to three dimensionality. For the four configurations vortex-adhesion mode and dislocations were highlighted and considered to be responsible for the bending of Karman vortices toward the horizontal position, leading to induced transient secondary flows. We suggested that this mechanism may explain the wavy distribution of the secondary flow in the lee side of the obstacles, particularly pronounced for the tapered case. In addition, cells of constant mean frequency were observed for the different configurations. It was shown that in the region with large variations of U/D cellular vortex pattern exhibited less variations in the size and position. Moreover, when spanwise distributions of U/D were larger, the size of the cells seemed to be broader and their number along the span was fewer.

Acknowledgments

Calculations were carried out at the IDRIS. This study was partially funded by the Région Poitou-Charentes.

References

[1] Balasubramanian, S., Haan, JR, F.L., Szewczyk, A.A. and Skop, R.A., 1998, On the existence of a critical shear parameter for cellular vortex shedding from cylinders in nonuniform flow. *Journal of Fluids and Structures*, **12**, 3–15.

[2] Balasubramanian, S., Haan, Jr, F.L., Szewczyk, A.A. and Skop, R.A., 2001, An experimental investigation of the vortex-induced vibrations of pivoted tapered circular cylinders in uniform and shear flow. *Journal of Wind Engineering and Industrial Aerodynamics*, **89**, 757–784.

[3] Braud, C., Heitz, D., Arroyo, G. and Delville, J., 2004, Analysis of the wake-mixing-layer interaction using multiple plane PIV and 3D classical POD. *Experiments in Fluids*, **37**, 95–104.

[4] Braud, C., Heitz, D., Arroyo, G., Perret, L., Delville, J. and Bonnet, J.-P., 2004, Low-dimensional analysis, using POD, for two mixing layer-wake interactions. *International Journal of Heat and Fluid Flow*, **25**, 351–363.

[5] Fey, U., König, M. and Eckelmann, H., 1998, A new Strouhal–Reynolds-number relationship for the circular cylinder in the range $47 < Re < 2 \times 10^5$. *Physics of Fluids* A, **10**(7), 1547–1549.

[6] Gaster, M., 1969, Vortex shedding from slender cones at low Reynolds numbers. *Journal of Fluid Mechanics*, **38**, 565–576.

[7] Gaster, M., 1971, Vortex shedding from circular cylinders at low Reynolds numbers. *Journal of Fluid Mechanics*, **46**, 749–.

[8] Gerrard, J.H., 1978, The wake of cylindrical bluff bodies at low Reynolds number. *Philosophical Transactions of the Royal Societies, Series* A, **288**(1354), 351–382.

[9] Griffin, O.M., 1985, Vortex shedding from bluff bodies in a shear flow: a review. *Journal of Fluids Engineering*, **107**, 298–306.

[10] Kappler, M., Rodi, W., Szepessy, S. and Badran, O., 2005, Experiments on the flow past long circular cylinders in a shear flow. *Experiments in Fluids*, **38**, 269–284.

[11] Lamballais, E. and Silvestrini, J.H., 2002, Direct numerical simulation of interactions between a mixing layer and a wake around a cylinder. *Journal of Turbulence*, **3**, 000–028.

[12] Lardeau, S., Lamballais, E. and Bonnet, J.-P., 2002, Direct numerical simulation of a jet controlled by fluid injection. *Journal of Turbulence*, **3**, 002.

[13] Lewis C.G. and Gharib, M., 1992, An exploration of the wake three dimensionalities caused by a local discontinuity in cylinder diameter. *Physics of Fluids*, **4**(1), 104–117.

[14] Mair, W.A. and Stansby, P.K., 1975, Vortex shedding from bluff cylinders in shear flow. *SIAM Journal of Applied Mathematics*, **28**, 519–540.

[15] Maull, D.J. and Young, R.A., 1973, Vortex shedding from bluff bodies in a shear flow. *Journal of Fluid Mechanics*, **60**(2), 401–409.

[16] Mukhopadhyay, A., Venogopal, P. and Vanka, S., 2002, Oblique vortex shedding from circular cylinder in linear shear flow. *Computer and Fluids*, **31**, 1–24.

[17] Noca, F., Park, H.G. and Gharib, M., Vortex formation length of a circular cylinder ($300 < Re < 4000$) using DPIV. In *FEDSM98–5149*, Washington DC, June 21–25 1998. ASME Fluids Engineering Division Summer Meeting.

[18] Papangelou, A., 1992, Vortex shedding from slender cones at low Reynolds numbers. *Journal of Fluid Mechanics*, **242**, 299–321.

Downloaded By: [Heitz, D.] At: 14:56 6 June 2007

[19] Parnaudeau, P., Lamballais, E., Heitz, D. and Silvestrini, J.H., 2003, Combination of the immersed boundary method with compact schemes for DNS of flows in complex geometry. In R. Friedriech, B. Geurts and O. Métais (Eds.) *Direct and Large-Eddy Simulation* (Dordrecht: Kluwer).

[20] Piccirillo, P.S. and Van Atta, C.W., 1993, An experimental study of vortex shedding behind linearly tapered cylinders at low Reynolds number. *Journal of Fluid Mechanics*, **246**, 163–195.

[21] Prasad, A. and Williamson, C.H.K., 1997, Three-dimensional effects in turbulent bluff-body wakes. *Journal of Fluid Mechanics*, **343**, 235–265.

[22] Provansal, M., Monkewitz, P. and Pruvost, L., 2005, Visualisations des vortex déversés dans le sillage d'un cÙne. In *Actes du Colloque FLUVISU11* (France: ECL, Ecully).

[23] Ramberg, S.E., 1983, The effects of yaw and finite length upon the vortex wakes of stationary and vibrating circular cylinders. *Journal of Fluid Mechanics*, **128**, 81–107.

[24] Silvestrini, J.H. and Lamballais, E., 2004, Direct numerical simulation of oblique vortex shedding from a cylinder in a shear flow. *International Journal of Heat and Fluid Flow*, **25**, 461–470.

[25] Vallès, B., Andersson, H.I. and Jenssen, C.B., 2002, Direct-mode interactions in the wake behind a stepped cylinder. *Physics of Fluids*, **14**(4), 1548–1551.

[26] Vallès, B., Andersson, H.I. and Jenssen, C.B., 2002, Oblique vortex shedding behind tapered cylinders. *Journal of Fluids and Structures*, **16**(4), 453–463.

[27] Williamson, C.H.K., 1992, The natural and forced deformation of spot-like 'vortex dislocations' in the transition of a wake. *Journal of Fluid Mechanics*, **243**, 393.

[28] Williamson, C.H.K., 1996, Three-dimensional wake transition. *Journal of Fluid Mechanics*, **328**, 345–407.

[29] Woo, H.G.C., Cermak, J.E. and Peterka, J.A., 1989, Secondary flows and vortex formation around a circular cylinder in constant shear flow. *Journal of Fluid Mechanics*, **204**, 523–542.

[30] Zhang, H.-Q., Fey, U., Noack, B., König, M. and Eckelmann, H., 1995, On the transition of the cylinder wake. *Physics of Fluids*, **7**(4), 779–794.